IEEE Access
Multidisciplinary : Rapid Review : Open Access Journal

Received July 30, 2019, accepted August 13, 2019, date of publication August 16, 2019, date of current version August 30, 2019.

Digital Object Identifier 10.1109/ACCESS.2019.2935735

Wideband Power Spectrum Estimation Based on Sub-Nyquist Sampling in Cognitive Radio Networks

YIJIU ZHAO[1], (Member, IEEE), YU CHEN[1], YANZE ZHENG[1], YI ZHUANG[1], AND WEIFENG WEN[2]

[1]School of Automation Engineering, University of Electronic Science and Technology of China, Chengdu 611731, China
[2]Institute of Fluid Physics, China Academy of Engineering Physics, Mianyang 621999, China

Corresponding author: Yijiu Zhao (yijiuzhao@uestc.edu.cn)

This work was supported in part by the National Natural Science Foundation of China under Grant 61671114, in part by the Sichuan Science and Technology Program under Grant 2019YJ0207, and in part by the Fundamental Research Funds for the Central Universities under Grant ZYGX2018J063.

ABSTRACT The wideband spectrum estimation is an essential step in the wireless network. In order to avoid employing power-hungry high-rate analog-to-digital converters (ADCs), the CS-based sub-Nyquist sampling approaches are used to estimate the wideband spectrum. In this paper, we propose a sub-Nyquist sampling system based on the analog to information converter (AIC), and the proposed system is constructed by multiple parallel channels with a banks of low pass filters. The system model is constructed in the time domain. To estimate the power spectrum, we define a new power spectrum of samples with a finite length, called the circular power spectrum (CPS), served as the aim we strive to estimate. The defined CPS can clearly reflect the power of the signal varying with frequency and is also with the same length as the equivalent digital samples. The experimental results indicate that the defined CPS can be successfully estimated from samples captured by the proposed sub-Nyquist sampling system whose overall sampling rate is much lower than the Nyquist rate.

INDEX TERMS Cognitive radio, power spectrum estimation, circular power spectrum, compressed sensing, sub-Nyquist sampling, wireless sensor network.

I. INTRODUCTION

In the wireless communication, the baseband signal is modulated to the high radio frequency (RF) band before being transmitted. In order to prevent the interference between transmitters, the government agencies assign the usage right of each RF band to a specific user (also called as the primary user: PU). The increasing demand of transmissions results in the RF spectrum scarcity problem. However, the PUs are not always active, and there are a large number of authorized subbands being unoccupied. It causes a large waste of spectrum resources and a very poor efficiency of the communication system. To solve this problem, a promising scheme called the cognitive radio (CR) is proposed [1]–[3], which can sense the RF spectrum and search for the transmission opportunities for the unlicensed users (also called as the second users: SUs) in real time. The CR technique significantly improves the utilization efficiency of RF spectrum. The spectrum sensing is the crucial step in CR. Many algorithms about the spectrum sensing are proposed in CR [4], [5]. However. the most of the previous works focus on detecting the status of the PUs, which are based on the obtained samples that are captured at the Nyquist rate. In practical, in order to detect the unused spectrum holes, CR has to monitor the RF spectrum at the Nyquist rate [4]. Generally, the band range of RF signal is wide, the power-hungry and high-rate analog-to-digital converters (ADCs) are required. On the other hand, due to the wideband features of the RF spectrum, the Nyquist rate of the signal of interest may exceeds the specifications of the best of the ADCs by orders of magnitude. The single high speed ADC solution cannot meet requirement of RF signal acquisition. To address this challenge, many alternative approaches have been proposed.

The time-interleaved sampling technique (TIS) is a famous and widely used method that are adopted to acquire high frequency signal in wireless communication system and radar

The associate editor coordinating the review of this article and approving it for publication was Rongbo Zhu.

system [6], [7]. The TIS samples the signal of interest using a banks of low-speed ADCs that are clocked at the rates with uniform phase delays. Obviously, the hardware implementation of TIS is complicated, and the input bandwidth of ADC limits the maximum frequency of the signal of interest. In comparison to TIS, the random equivalent sampling (RES) technique would be relatively simple [8]. The RES use only one low speed ADC to acquire high speed signal. In order to capture enough information, multiple RES sampling sequences has to be obtained. In the process of acquisition, the signal should remain unchanged, and a unique trigger reference should be provide in each acquisition. Clearly, there are much more limitation of RES application. The TIS and RES pay no attention to the inherent feature of the signal of interest. The Nyquist sampling is not necessary in many applications, such as sparse signal acquisition, where the signal information rate is much lower than its band range. For this kind of signal acquisition, more intelligent ways can be employed.

Compressed sensing (CS) has been proposed as an intelligent signal processing theory for the inherent sparse signal [9], [10]. According to the CS theory, sampling at the Nyquist rate is not necessary if the signal is sparse in a certain domain. To be specific, we can sample a sparse wideband signal at a rate much lower than its Nyquist rate and subsequently recover the original signal from a small number of low-rate samples. Since it is proposed, the CS theory has been widely studied in the fields of imaging signal processing, wireless communication *et. al*. In this work, we focus on the CS application in the spectrum sensing of the wireless communication system.

The CS theory make the promise that the original signal can be successfully recovered from a small number of samples, which are captured by the ADCs that are clocked at the sub-Nyquist rates. Since the wireless sensor network (WSN) is sensitive to the energy, the feature of CS theory is suitable for WSN signal processing, and the CS theory has found many applications in WSN [11]–[13]. In WSN application, a large number of well-distributed sensors are used to monitor the environment, such as signal spectrum [14]. Fortunately, the signal of interest in WSN has been exploited to be sparse in some basis. With the help of CS, a relatively small number of low rate samples are obtained. It's very meaningful in WSN, small number of WSN samples means the minimization of storage and communication in WSN nodes, and low rate samples means power-hungry high speed ADCs are not required. The application of CS in WSN can extend the lifetime of the sensor nodes. Another application of CS in WSN is the estimation directions-of-arrival (DOA) in the spatial domain. In the DOA estimation, high sampling rate can achieve high resolution, the node with high speed ADC is adopted in the traditional WSN. To improve the DOA estimation accuracy, the CS theory has been employed in WSN [15], [16]. CS extracts the signal information from a small number of low rate samples and recovery signal with the high equivalent sampling rate, and it increases the degree of freedom and improve the estimation accuracy.

In the CS framework, many approaches are also developed to decrease the sampling rate, and sparse reconstruction algorithms are proposed to recover the original signal [17]–[19]. In these sub-Nyquist sampling approaches, The most popular ways are analog to information converter (AIC) [20], [21] and modulated wideband converter (MWC) [22], both of which are based on the random demodulation (RD) technique. Since only the base band signal is sampled, the RD-based approaches not only achieve the sub-Nyquist sampling but also avoid the bandwidth limitation of ADCs, and they can realize the compression in the sampling stage. Base on CS theory, some other sub-Nyquist sampling methods are also developed. By incorporating CS to RES technique. CS-based RES can reduce the requirement of number of RES acquisitions [23], and the limitation of input bandwidth of ADCs can be avoided [24]. In [25], the quadrature AIC (QAIC) employs frequency down-conversion to decrease the number of sampling channels of MWC. Some other sub-Nyquist sampling approaches are also proposed [26]–[29], however, they suffer from the bandwidth limitation of ADCs.

All the above sampling approaches are aimed at recovering the original signal or the signal spectrum. However, in CR, the SUs make the decision of transmission base on the absence of PUs, and the signal spectrum recovery is not required and the signal power spectrum or power spectral density is enough. In [30], a power spectrum estimation system based on multicoset sampling is proposed, which however does not avoid the disadvantages of the inherent bandwidth limitation of ADCs and the accuracy of time shift. In [31], the signal power spectrum is estimated based on the parallel AIC model. However, it employs a bank of integrators which have to be reset in each sampling period. The reset process is non-trivial in practice, and it may limit the application of AIC [32]. In this paper, we employ the low pass filters instead of integrators to propose an AIC-based system to estimate wideband power spectrum by low-rate ADCs. The low pass filter is represented by a toeplitz matrix and the proposed system is constructed in time domain. In our proposed model, the low pass filter is assumed to be ideal. Different from other power spectrum estimation approaches, we define a circular autocorrelation function (AF) and circular power spectrum (CPS) of samples with finite length. The definition can reflect signal's power with respect to the frequency and is appropriate to the proposed system. According to the circular cross-correlation between outputs of different channels, the CPS can be recovered using least squares (LS) or traditional CS recovery algorithms. Note that the assumption on signal sparsity is not necessary in the proposed system, provided that the number of channels is big enough to the given compression rate.

The rest of paper is organized as follows. The sub-Nyquist sampling system is proposed in Section II. The definition

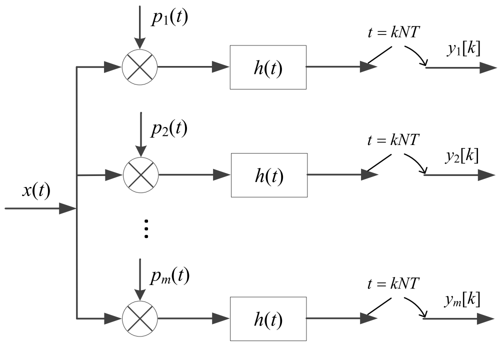

FIGURE 1. The block diagram of the proposed sampling system with m channels.

of CPS is given and the relationship between the CPS of the input and the circular cross-correlation of the outputs is derived in Section III. The power spectrum estimation model is proposed in Section IV. The comparison is give in Section V. And the simulation results are reported in Section VI, followed by the conclusion in Section VII.

II. THE SUB-NYQUIST SAMPLING MODEL

Our aim is to sense wideband power spectrum of RF signals, so we assume that the input signal denoted by $x(t)$ is a stationary wideband but bandlimited real-valued signal with the Nyquist rate of $1/T$.

As shown in Fig. 1, the system is a period-modulation sub-Nyquist sampling system consisting of multiple channels. Specifically, in ith channel, $x(t)$ is firstly modulated in the mixer by a NT-periodic random signal $p_i(t)$, which stochastically alternates at the Nyquist rate of $1/T$ between the levels ± 1 in each period. Then the modulated wideband signal is filtered by a low-pass filter (LPF) with cutoff $1/(2NT)$ denoted by $h(t)$. Finally, the baseband signal is sampled by a low-rate ADC with the sampling interval NT. Note that the modulation signal $p_i(t)$ in each channel is different from each other, so we can obtain m distinct measurement vectors from m channels. N is called the sub-Nyquist factor, and m/N is the compression rate. The overall sampling rate of the system is m/NT. The sub-Nyquist sampling can be achieved if $m < N$. Consider the ith channel, its output can be expressed as

$$y_i[k] = \int_{-\infty}^{+\infty} x(\tau)p_i(\tau)h(t-\tau)\mathrm{d}\tau|_{t=kNT}. \tag{1}$$

According to the sampling model, the relation between the measurement vector $\mathbf{y}_i$ of length M of the ith channel and the input signal that is expressed as its equivalent Nyquist sampling sequence $\mathbf{x}$ of length $L(L = NM)$, which can be expressed as the vector-matrix form

$$\mathbf{y}_i = \mathbf{RHP}_i\mathbf{x}, \tag{2}$$

where $\mathbf{R}$ is an $M \times L$ downsampling matrix, $\mathbf{H}$ is an $L \times L$ toeplitz matrix denoting the operation of the low-pass filter and $\mathbf{P}_i$ is an $L \times L$ diagonal period-modulation matrix. More specifically, the entry of jth row and jNth column of $\mathbf{R}$ is equal to 1 ($1 \leq j \leq M$), and other entries are 0. An example with $N = 3$ is

$$\mathbf{R} = \begin{bmatrix} 0 & 0 & 1 & & & & & & & \\ & & & 0 & 0 & 1 & & & & \\ & & & & & & \ddots & & & \\ & & & & & & & 0 & 0 & 1 \end{bmatrix}. \tag{3}$$

Denote by $\mathbf{h}$ the L consecutive impulse response samples of low-pass filter, and $\mathbf{h} = [h_1, h_2, \ldots, h_L]^T$. In this paper, we consider the ideal low-pass filter, and $\mathbf{h}$ has the symmetrical structure. The Toeplitz matrix $\mathbf{H}$ models the operation of the low-pass filter. It has the form as

$$\mathbf{H} = \begin{bmatrix} h_1 & h_L & h_{L-1} & \cdots & h_2 \\ h_2 & h_1 & h_L & \ddots & h_3 \\ h_3 & h_2 & h_1 & \ddots & h_4 \\ \vdots & \vdots & \vdots & \ddots & \vdots \\ h_L & h_{L-1} & h_{L-2} & \cdots & h_1 \end{bmatrix}. \tag{4}$$

The modulation matrix $\mathbf{P}_i$ can be expressed as

$$\mathbf{P}_i = \mathbf{I}_M \otimes \mathbf{D}_i, \tag{5}$$

where $\mathbf{I}_M$ is an identity matrix with dimension M equal to the length of measurement vector of each channel, $\mathbf{D}_i$ is an $N \times N$ diagonal matrix whose diagonal entries are equal to $+1$ or -1 with the same probability 1/2 and "$\otimes$" denotes the Kronecker product. As an example, the diagonal entries of the $\mathbf{D}_i$ denoted by $[a_1, a_2, \ldots, a_N]$ (the value of entry is $+1$ or -1) is

$$\mathbf{P}_i = diag(a_1, a_2, \ldots, a_N, a_1, a_2, \ldots, a_N, \ldots, a_1, a_2, \ldots, a_N). \tag{6}$$

Reverse the diagonal vector of $\mathbf{P}_i$, we obtain a sequence $\mathbf{a}_i$ and construct matrix $\mathbf{Q}_i = diag(\mathbf{a}_i)$. Since $\mathbf{H}$ is the toeplitz matrix, the $(l+1)$th row is the circularly right shifted vector of the lth row. Denote by $\mathbf{c}_i = \mathbf{hQ}_i$ a digital filter operation, we can define an observation $\mathbf{z}_i$ as

$$z_i[l] = c_i[l] \circledast x[l], \tag{7}$$

where "$\circledast$" denotes the circular convolution operator, $1 \leq l \leq L$. Therefore, the output $\mathbf{y}_i$ can be viewed as the N-fold downsampling version of $\mathbf{z}_i$, and

$$y_i[k] = z_i[kN], \tag{8}$$

where $1 \leq k \leq M$.

III. CIRCULAR POWER SPECTRUM

The bandlimited signals are infinite in time domain. Although the processed signals are assumed to be bandlimited, the observation time must be finite, i.e., the original signal $x[l]$ we strive to recover and the samples $y_i[k]$ we actually obtained are both finite-length sequences. Nevertheless, the common definition of AF is given over infinite timescale, i.e., $r_x[k] = \mathrm{E}\{x[l]x[l\text{-}k]\}$, where $l, k \in \mathbb{Z}$. If this definition

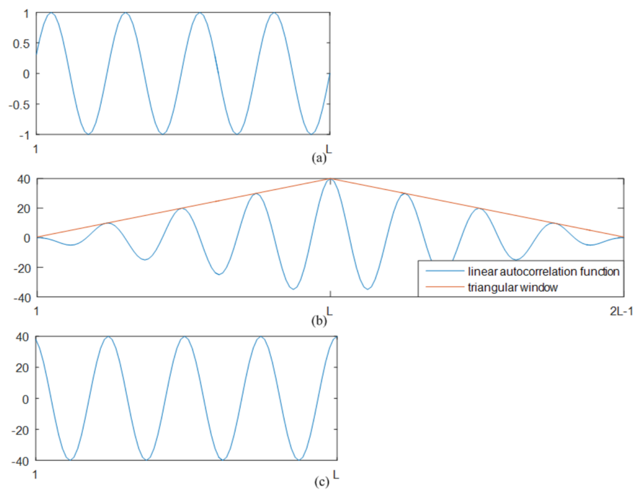

FIGURE 2. **(a) is a sinusoidal wave of length L. (b) is its linear autocorrelation as well as the triangular window. (c) is its circular autocorrelation.**

is directly employed in the situation of finite-length signals, we will obtain a truncated AF, called linear AF. And the linear AF of the finite-length sequence $x[k]$ of length L is defined as

$$r_x^l[k] = \sum_l x[l]x[l-k], \quad l, l-k \in [1, L]. \tag{9}$$

Due to the impact of truncation, the length of $r_x^l[k]$ is changed to $2L$-1 and a triangular window is added to $r_x^l[k]$. A prime example of finite-length sinusoidal signal is shown in Fig. 2. As we know, the AF of an infinite-length sinusoidal wave is also an infinite-length sinusoidal wave with the same frequency. However, it is clear in Fig. 2 (b) that the linear AF is no longer a standard sinusoidal wave. And it is derived from an infinite-length sinusoidal wave truncated by a triangular window of length L. This triangular window can be expressed as

$$w(t) = \begin{cases} LT - t, & t \in [0, LT] \\ LT + t, & t \in [-LT, 0] \end{cases}. \tag{10}$$

The Fourier Transform of $w(t)$ denoted by $W_t(\omega)$ can be calculated as:

$$\begin{aligned} W_t(\omega) &= \int_{-\infty}^{+\infty} w(t)e^{-j\omega t}dt \\ &= LT\int_{-LT}^{LT} e^{-j\omega t}dt + \int_{-LT}^{0} te^{-j\omega t}dt - \int_{0}^{LT} te^{-j\omega t}dt \\ &= 2L^2T^2 \cdot \sin c(\frac{\omega LT}{\pi}) + \frac{1}{-j\omega}(te^{-j\omega t}\Big|_{-LT}^{0} - te^{-j\omega t}\Big|_{0}^{LT}) \\ &\quad + \frac{1}{j\omega}(\int_{-LT}^{0} e^{-j\omega t}dt - \int_{0}^{LT} e^{-j\omega t}dt) \\ &= 2L^2T^2 \cdot \text{sinc}(\frac{\omega LT}{\pi}) - 2L^2T^2 \cdot \text{sinc}(\frac{\omega LT}{\pi}) \\ &\quad + L^2T^2 \cdot \text{sinc}^2(\frac{\omega LT}{2\pi}) \\ &= L^2T^2 \cdot \text{sinc}^2(\frac{\omega LT}{2\pi}) \end{aligned} \tag{11}$$

where

$$\sin c(x) = \begin{cases} 1, & x = 0 \\ \dfrac{\sin(\pi x)}{x}, & \text{others} \end{cases}.$$

The interval of zero-crossing points of $W_t(\omega)$ is $4\pi/LT$. By contrast, the Fourier Transform of rectangular window is $W(\omega) = 2LT \cdot \text{sinc}(\omega LT/\pi)$ whose interval of zero-crossing points is $2\pi/LT$. Assuming $L = 10$, $W_t(\omega)$ and $W(\omega)$ are shown in Fig. 2. Their discrete forms, i.e. discrete Fourier transform (DFT) of the two windows, must be also considered. As shown in Fig.2, all the zero-crossing points of $W(\omega)$ and $W_t(\omega)$ are exactly located in integer points as long as the main frequency of $W(\omega)$ is located in an integer point. However, there always exist non-zero harmonic components in DFT of the triangular window no matter where its main frequency is. The sparsity of signal in frequency domain will be certainly increased by these non-zero harmonic components, especially the two significant components at the both sides of the main frequency. This could have a marked impact on the signal recovery because most CS algorithm is base on the sparsity of signals. The other disadvantage of this triangular window is noticeable. The window length of linear AF is nearly twice the window length of its original signal, which enormously increases the difficulty of computation and storage.

To conquer these two problems, the circular AF of finite-length sequences is proposed. Similar to the relationship between the linear convolution and the circular convolution, the circular AF of the finite-length sequence $x[k]$ of length L can be defined by its linear AF $r_x^l[k]$, shown as

$$r_x^c[k] = \begin{cases} r_x^l[k] + r_x^l[k-L], & k \in (1, L] \\ r_x^l[k], & k = 1 \end{cases}. \tag{12}$$

Still using the example of finite-length sinusoidal wave, its circular AF is shown in Fig. 2 (c). As we can see, it is exactly the infinite-length AF truncated by the same rectangular window as the one added in signal. As shown in Fig. 3 (b), the DFT of rectangular windows have no non-zero harmonic components if its main frequency is located in an integer point. Even if not, i.e., spectrum leakage happens, the relative amplitudes of its non-zero harmonic components are still much smaller than the relative amplitudes of harmonic components of triangular window at the both sides of the main frequency. So this rectangular window has smaller impact on sparsity than the triangular window in linear AF. Moreover, circular AF has the same length as the finite-length signal, which is superior to linear AF in signal storage and processing.

According to the DFT of $r_x^c[k]$, we define the CPS of the finite-length sequence $x[k]$ of length L as

$$P_x^c[k] = \text{DFT}\left(r_x^c[k]\right). \tag{13}$$

The defined P_x^c, also a finite-length sequence of the same length as $x[k]$, is easy for the digital signal processer to

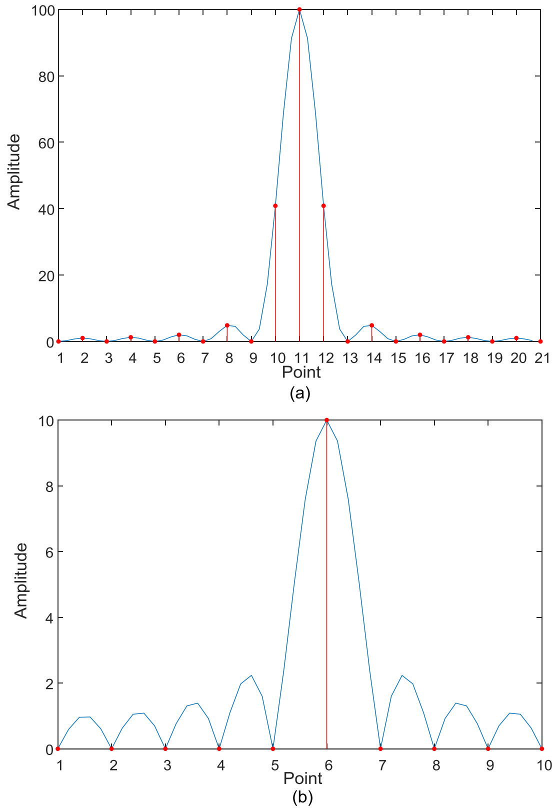

FIGURE 3. **(a) is the frequency spectrum of triangular window as well as its discrete values in DFT and (b) is the frequency spectrum of rectangular window as well as its discrete values in DFT. Here we assume L = 10.**

deal with. More significantly, signals' power varying with frequency can be clearly reflected by the $r_x^l[k]$, also given by $\left|P_x^c[k]\right| = |DFT(x[k])|^2/L$.

Similar to the definitions of the linear AF and the circular AF of a finite-length sequence, the linear cross-correlation function and the circular cross-correlation function between $y_i[k]$ and $y_j[k]$ are respectively defined as

$$r^l_{y_i,y_j}[k] = \sum\nolimits_l y_i[l]y_j[l-k], \quad l, l-k \in [1, M], \tag{14}$$

and

$$r^c_{y_i,y_j}[k] = \begin{cases} r^l_{y_i,y_j}[k] + r^l_{y_i,y_j}[k-M], & k \in (1, M] \\ r^l_{y_i,y_j}[k], & k = 1 \end{cases}. \tag{15}$$

IV. POWER SPECTRUM ESTIMATION

In the proposed system with m channels, $(m+1)m/2$ different circular cross-correlation functions can be exploited. In order to recover signal power spectrum, we need to derive the relation between the circular cross-correlation function of the outputs and the circular autocorrelation $r_x^c[k]$.

According to (7) and (8), the circular cross-correlations of the $\mathbf{z}_i$ can be expressed as

$$r^c_{z_i,z_j}[k] = r^c_{c_i,c_j}[k]| \circledast r^c_x[k], \tag{16}$$

and

$$\begin{aligned} r^c_{y_i,y_j}[k] &= \frac{1}{N} r^c_{z_i,z_j}[kN] \\ &= \frac{1}{N} r^c_{c_i,c_j}[kN] \circledast r^c_x[kN]. \end{aligned} \tag{17}$$

We can re-write (17) in the vector-matrix form as

$$\mathbf{r}^c_{y_i,y_j} = \frac{1}{N}\mathbf{D} \cdot \mathbf{C}_{i,j} \cdot \mathbf{r}^c_x, \tag{18}$$

where $\mathbf{r}^c_{y_i,y_j} = [r^c_{y_i,y_j}[1], r^c_{y_i,y_j}[2], \cdots, r^c_{y_i,y_j}[M]]^T$, $\mathbf{r}^c_x = [r^c_x[1], r^c_x[2], \cdots, r^c_x[L]]^T$, $\mathbf{D}$ is an $M \times L$ downsampling matrix similar to $\mathbf{R}$, and $\mathbf{C}_{i,j}$ is the $L \times L$ Toeplitz matrix with the expression as

$$\mathbf{C}_{i,j} = \begin{bmatrix} r^c_{c_i,c_j}[1] & r^c_{c_i,c_j}[L] & r^c_{c_i,c_j}[L-1] & \cdots & r^c_{c_i,c_j}[2] \\ r^c_{c_i,c_j}[2] & r^c_{c_i,c_j}[1] & r^c_{c_i,c_j}[L] & \cdots & r^c_{c_i,c_j}[3] \\ r^c_{c_i,c_j}[3] & r^c_{c_i,c_j}[2] & r^c_{c_i,c_j}[1] & \cdots & r^c_{c_i,c_j}[4] \\ \vdots & \vdots & \vdots & \ddots & \vdots \\ r^c_{c_i,c_j}[L] & r^c_{c_i,c_j}[L-1] & r^c_{c_i,c_j}[L-2] & \cdots & r^c_{c_i,c_j}[1] \end{bmatrix}. \tag{19}$$

Consider all the m channels in the proposed system to obtain $(m+1)m/2$ different equations as (18). Combine these equations in a certain order to obtain

$$\begin{bmatrix} \mathbf{r}^c_{y_1,y_1} \\ \mathbf{r}^c_{y_1,y_2} \\ \vdots \\ \mathbf{r}^c_{y_1,y_m} \\ \mathbf{r}^c_{y_2,y_2} \\ \mathbf{r}^c_{y_2,y_3} \\ \vdots \\ \mathbf{r}^c_{y_2,y_m} \\ \vdots \\ \mathbf{r}^c_{y_m,y_m} \end{bmatrix} = \frac{1}{N} \begin{bmatrix} \mathbf{D} \cdot \mathbf{C}_{1,1} \\ \mathbf{D} \cdot \mathbf{C}_{1,2} \\ \vdots \\ \mathbf{D} \cdot \mathbf{C}_{1,m} \\ \mathbf{D} \cdot \mathbf{C}_{2,2} \\ \mathbf{D} \cdot \mathbf{C}_{2,3} \\ \vdots \\ \mathbf{D} \cdot \mathbf{C}_{2,m} \\ \vdots \\ \mathbf{D} \cdot \mathbf{C}_{m,m} \end{bmatrix} \cdot \mathbf{r}^c_x,$$

$$\Leftrightarrow \mathbf{r}^c_{\mathbf{y},\mathbf{y}} = \mathbf{\Phi} \cdot \mathbf{r}^c_x, \tag{20}$$

where $\mathbf{r}^c_{\mathbf{y},\mathbf{y}}$ is the $M(m+1)m/2 \times 1$ vector, and $\mathbf{\Phi}$ is $M(m+1)m/2 \times L$ matrix. Combine (13), eqn. (20) can be re-written as

$$\mathbf{r}^c_{\mathbf{y},\mathbf{y}} = \mathbf{\Phi} \cdot \mathbf{\Psi} \cdot \mathbf{P}^c_x. \tag{21}$$

where $\mathbf{\Psi}$ is the $L \times L$ inverse DFT matrix and $\mathbf{P}^c_x$ is a $L \times 1$ vector denoting the circular power spectrum $P^c_x[k]$.

Note from (21), it is a underdetermined problem in the case $M(m+1)m/2 < L$, i.e. when the number of channels m is small. Because the measurement matrix $\mathbf{\Phi}$ is a random matrix constructed by m different periodic random modulating sequences whose periods are equal to the sub-sample factor N, and $\mathbf{\Phi}$ satisfies the restricted isometry property (RIP) with high possibility as N increases. With the additional constraint of sparsity on $\mathbf{P}^c_x$, problem (21) becomes a standard mathematic model of CS literature, making the perfect recovery of $\mathbf{P}^c_x$ possible in the case of $M(m+1)m/2 < L$.

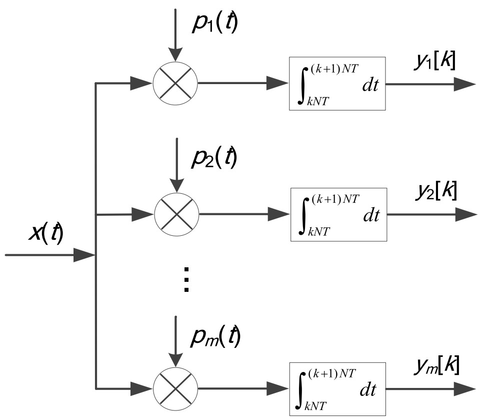

FIGURE 4. The block diagram of the integrator-based sampling system with m channels.

Since $L = NM$, eqn. (23) can be transformed into an overdetermined problem with a proper sub-sample factor N. Therefore, $\mathbf{P}_x^c$ can be estimated using the least square (LS) algorithm without any constraints on signals.

V. COMPARISON WITH THE RELATED WORK

In [18], a typical sub-Nyquist system can be used to estimate the linear power spectrum which is defined as the DFT of the linear AF, i.e.,

$$P_x^l[k] = \mathrm{DFT}\left(r_x^l[k]\right). \tag{22}$$

As illustrated in Fig. 4, this system employs a bank of integrators which have to be reset in each sampling period. The reset process is non-trivial in practice, and it may limit the practical performance of this system. The power spectrum estimation model of this system can be expressed as [17]

$$\mathbf{r}_{\mathbf{y},\mathbf{y}}^l = \mathbf{\Phi}^l \cdot \mathbf{\Psi} \cdot \mathbf{P}_x^l, \tag{23}$$

where $\mathbf{r}_{\mathbf{y},\mathbf{y}}^l$ denotes a $(2M-1)(m+1)m/2 \times 1$ vector composed of the linear correlation functions of sampling sequences in m channels, $\mathbf{P}_x^l$ denotes a $(2L-1) \times 1$ vector of linear power spectrum of input signal $x(t)$, $\mathbf{\Phi}^l$ denotes the $(2M-1)(m+1)m/2 \times (2L-1)$ measurement matrix composed of linear correlation functions of random sequence $p_i(t)$, and $\mathbf{\Psi}$ is the $(2L-1) \times (2L-1)$ inverse DFT matrix.

Compare (21) and (23), they have the same form. However, as regards the same input $x(t)$, sampling frequency and sampling time, $\mathbf{r}_{\mathbf{y},\mathbf{y}}^l$ and $\mathbf{P}_x^l$ are nearly twice longer than $\mathbf{r}_{\mathbf{y},\mathbf{y}}^c$ and $\mathbf{r}_x^c$ respectively, and $\mathbf{\Phi}^l$ is nearly 4 times bigger than $\mathbf{\Phi}$. This means that the computation amount of solving (23) is much bigger than the computation amount to solve (21) using the same algorithm. In addition, CS-based algorithms are not quite suitable for (23) due to the effect of triangular window on linear AF.

The differences between the proposed system in this paper and the integrator-based system are concluded in TABLE 1.

TABLE 1. Comparison between filter-based system (FS) and integrator-based system (IS).

Sampling approach	FS	IS
Structure	Filter-based	Integrator-based
Applicable correlation function	Circular	Linear
Computation amount	Small	Big
Applicable algorithm	Both LS and CS	LS
Applicable signal	Both multitone and passband signal	Both multitone and passband signal

VI. SIMULATION RESULTS

In this section, the numerical simulations are performed to evaluate the proposed system with different m/N, L, input signal-to-noise ratio (SNR) and sparsity K. And it is assumed that the noise added to the input is always white Gaussian noise in all the experiments. Served as a metric evaluating the recovery performance, the normalized mean square error (NMSE) between the input CPS and the recovered CPS is defined as

$$NMSE = \frac{\left\| \mathbf{P}_x^{c'} - \mathbf{P}_x^c \right\|}{\left\| \mathbf{P}_x^c \right\|}, \tag{24}$$

where the vector $\mathbf{P}_x^c$ denotes the CPS of the input signal without noise, the vector $\mathbf{P}_x^{c'}$ denotes the recovered CPS and the $|| \cdot ||$ denotes the Euclidean norm. In VI-A and VI-B, a bandpass signal with frequency support between 1.28 GHz and 1.32 GHz is tested. And in VI-C, a multitone signal with all frequency components verifying below 1.8 GHz is served as the input signal. To simplify, the discrete-time signal with the equivalent sampling rate of 3.6 GHz is generated.

A. CPS RECOVERY

In this subsection, we investigate the feasibility of the power spectrum estimation based on the defined CPS. $L = 1440$ equivalent samples are considered in this simulation. Fig.5(a) shows the amplitude-frequency curve (AFC) based on DFT of signal, Fig.5(b) shows the linear power spectrum (LPS) defined as (22). Obviously, for a sampling sequence with length of L, its LPS has the length of $2L-1$. So the system needs to store and process large number of data. By contrast, in the Fig.5(c), the CPS has the same length as the samples, and its values perfectly satisfy the relation $\left|P_x^c[k]\right| = |DFT(x[k])|^2/L$. Fig.5(d) shows the estimated CPS from the noise-free samples, which are acquired by the proposed system with $m = 6$ channels and the sub-Nyquist factor $N = 12$. The orthogonal matching pursuit (OMP) algorithm is used [6], and the estimated CPS achieves NMSE of 3.7×10^{-8}. Clearly, the feasibility of the proposed CPS estimation algorithm is demonstrated.

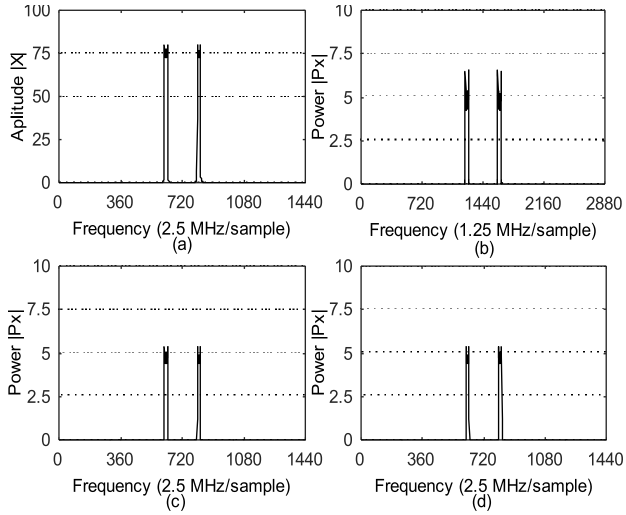

FIGURE 5. **(a) is the ACF of the input, (b) is the LPS of the input, (c) is CPS of the input, and (d) is the recovered CPS.**

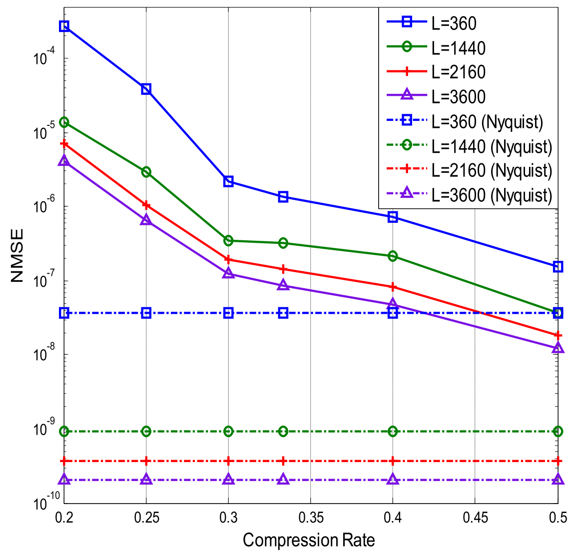

FIGURE 6. **The NMSE between the CPS of the input without noise and the recovered CPS with different m/N and L.**

B. CPS ESTIMATION OF BANDPASS SIGNAL

In this subsection, two experiments are carried out. In the first one, we consider the recovery performance in the noise-free environment with different sequence length L and compression rate m/N. To generate different m/N, we fix $m = 6$ and change N from 12 to 30. So the overall sampling rate is from 0.72 GHz to 1.8 GHz, which is much lower than the Nyquist sampling rate of 3.6 GHz. The underdetermined cases exist in the experiment due to the fact that m is relatively small. So the OMP algorithm is adopted to estimate the CPS. For each specific compression rate, 200 random trials are performed, and the averaged NMSEs are plotted in the Fig.6. the NMSE increases with the compression rate m/N decreasing while it gradually decreases with the sequence length L increasing. Set $m = N = 6$, the overall sampling rate achieves the Nyquist sampling rate. The horizontal lines in the Fig. 6 denote the NMSE of estimation from the "Nyquist" samples. These lines can be regarded as benchmarks reflecting the impact from sub-Nyquist sampling.

In practical application, the signal may be corrupted by noise. So, in the second experiment of this subsection, more practical situation is considered that the test signal is corrupted by the white Gaussian noise. In the simulation, $m = 6$ and $L = 3600$ are fixed, the compression rates over range of 0.2 to 0.5 in increment of 0.05 are tested in the noisy environment with different input SNRs. The OMP algorithm is used to estimate the CPS, and the averaged NMSEs from 200 random trials are depicted in Fig. 7. We still draw the benchmarks denoting the Nyquist sampling. In comparison to Fig. 6, the differences between the benchmarks and the NMSEs of estimation from sub-Nyquist samples are much smaller. This suggests that, for sub-Nyquist sampling, the impact on the estimation performance in the noise case is stronger than that of the noise-free case.

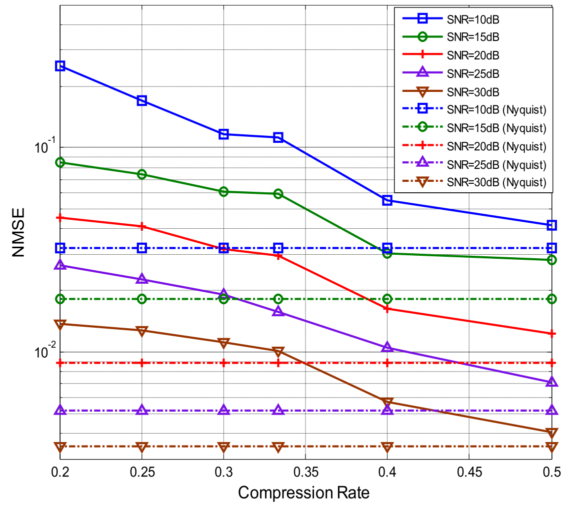

FIGURE 7. **The NMSE between the CPS and the recovered CPS with different m/N and input SNR.**

C. CPS ESTIMATION OF MULTITONE SIGNAL

As regards multitone signals, two experiments are conducted in this subsection, to compare the PS estimation performance and the support recovery performance of FS and IS. Here we set $L = 3600$, $m = 6$ and $N = 12$. The sparsity K varies from 2 to 6 and the input SNR varies from -30 dB to 30 dB. And all the frequency components of the multitone signal are random uniformly distributed from 0 to 1.8 GHz.

In the first experiment, the LS is chosen as the recovery algorithm and NMSE is still served as the criterion of their estimation performance. As illustrated in Fig. 8, the NMSE of both FS and IS decreases with input SNR increasing or sparsity K decreasing. The estimation performances of both FS and IS are acceptable only when input SNR exceeds 0 dB. When K is small, FS performs better than IS. Although the NMSE of FS is larger than the NMSE of IS in large-sparsity case, but it is still tolerable when input SNR exceeds 6 dB.

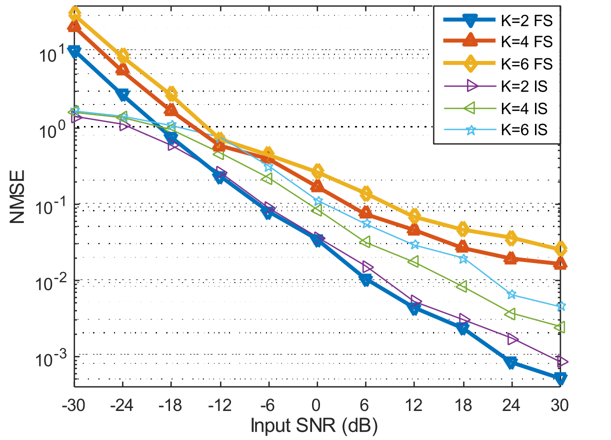

FIGURE 8. The NMSE of FS and IS with different sparsity K and input SNR.

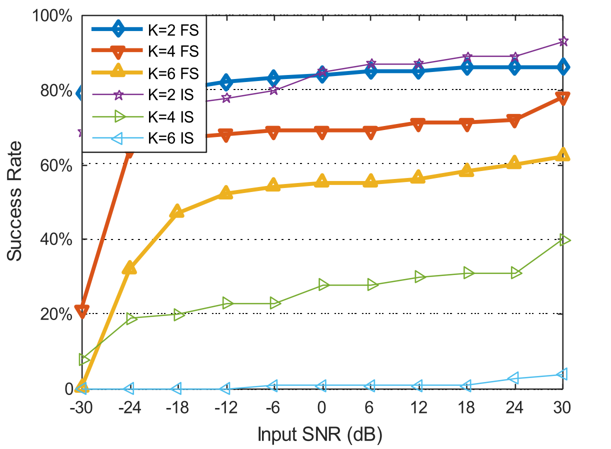

FIGURE 9. The support recovery rate of FS and IS with different sparsity K and input SNR.

Other than the error in the estimated outcome, it is also noteworthy whether the support of input signals can be found exactly. So in the second experiment, we use OMP algorithm to search for the support in the frame of PS estimation. 300 experiments are conducted in order to obtain the success rate of support recovery. As shown in Fig. 9, FS can reliably find the support when input SNR exceeds -18 dB which is a rather strong noise environment. However, due to the triangular window discussed in III, IS cannot precisely find the support expect the case of low sparsity level.

VII. CONCLUSION

In the paper, employing the time-domain model of low pass filters, we propose an AIC-based sub-Nyquist sampling system to estimate wideband power spectrum, which is the crucial step in wireless network or CR. We give a novel definition of power spectrum of finite-length sequences called circular power spectrum. The defined CPS can clearly reflect the power of the signal varying with frequency and it is also with the same length as original sequence making signal processing easier. Thanks to no triangular window added in the circular AF, CPS is superior to LPS in terms of the capability to remain the sparsity. Through mathematic derivation and experimental verification, the defined CPS can be exactly reconstructed even if the overall sampling rate is much lower than the Nyquist sampling rate. Moreover, compared with IS, FS has the similar PS estimation performance but in terms of support recovery, FS is much superior to IS. In order to make the system more practical, our future work is to study the ways to replace the ideal low pass filters by actual non-ideal low pass filters and analyze the impact on the recovery performance.

REFERENCES

[1] Y. Ma, Y. Gao, Y.-C. Liang, and S. Cui, "Reliable and efficient sub-Nyquist wideband spectrum sensing in cooperative cognitive radio networks," *IEEE J. Sel. Areas Commun.*, vol. 34, no. 10, pp. 2750–2762, Oct. 2016.

[2] Z. Qin, J. Wang, J. Chen, and L. Wang, "Adaptive compressed spectrum sensing based on cross validation in wideband cognitive radio system," *IEEE Syst. J.*, vol. 11, no. 4, pp. 2422–2431, Dec. 2017.

[3] Y. He, J. Xue, T. Ratnarajah, M. Sellathurai, and F. Khan, "On the performance of cooperative spectrum sensing in random cognitive radio networks," *IEEE Syst. J.*, vol. 12, no. 1, pp. 881–892, Mar. 2016.

[4] T. Xiong, Y.-D. Yao, Y. Ren, and Z. Li, "Multiband spectrum sensing in cognitive radio networks with secondary user hardware limitation: Random and adaptive spectrum sensing strategies," *IEEE Trans. Wireless Commun.*, vol. 17, no. 5, pp. 3018–3029, May 2018.

[5] D. Sun, T. Song, B. Gu, X. Li, J. Hu, and M. Liu, "Spectrum sensing and the utilization of spectrum opportunity tradeoff in cognitive radio network," *IEEE Commun. Lett.*, vol. 20, no. 12, pp. 2442–2445, Dec. 2016.

[6] F. M. C. Clemencio, C. F. M. Loureiro, and C. M. B. A. Correia, "An easy procedure for calibrating data acquisition systems using interleaving," *IEEE Trans. Nucl. Sci.*, vol. 54, no. 4, pp. 1227–1231, Aug. 2007.

[7] V. G. Ivchenko, A. N. Kalashnikov, R. E. Challis, and B. R. Hayes-Gill, "High-speed digitizing of repetitive waveforms using accurate interleaved sampling," *IEEE Trans. Instrum. Meas.*, vol. 56, no. 4, pp. 1322–1328, Aug. 2007.

[8] R. A. Witte, "Sample rate and display rate in digitizing oscilloscopes," *Hewlett-Packward J.*, vol. 43, no. 1, pp. 18–19, Feb. 1992.

[9] E. J. Candès, J. Romberg, and T. Tao, "Robust uncertainty principles: Exact signal reconstruction from highly incomplete frequency information," *IEEE Trans. Inf. Theory*, vol. 52, no. 2, pp. 489–509, Feb. 2006.

[10] D. L. Donoho, "Compressed sensing," *IEEE Trans. Inf. Theory*, vol. 52, no. 4, pp. 1289–1306, Apr. 2006.

[11] Z. Zhang, X. Wen, H. Xu, and L. Yuan, "Sensing nodes selective fusion scheme of spectrum sensing in spectrum-heterogeneous cognitive wireless sensor networks," *IEEE Sensors J.*, vol. 18, no. 1, pp. 436–445, Jan. 2018.

[12] C.-H. Chen and J.-Y. Wu, "Amplitude-aided 1-bit compressive sensing over noisy wireless sensor networks," *IEEE Wireless Commun. Lett.*, vol. 4, no. 5, pp. 473–476, Oct. 2015.

[13] X. Yang, X. Tao, E. Dutkiewicz, X. Huang, Y. Guo, and Q. Cui, "Energy-efficient distributed data storage for wireless sensor networks based on compressed sensing and network coding," *IEEE Trans. Wireless Commun.*, vol. 12, no. 10, pp. 5087–5099, Oct. 2013.

[14] W. Xue, J. Min, X. Gu, and Q. Guo, "Sub-Nyquist spectrum sensing based on modulated wideband converter in cognitive radio sensor networks," *IEEE Access*, vol. 6, pp. 40411–40419, 2018.

[15] L. Xu, R. Wu, X. Zhang, and Z. Shi, "Joint two-dimensional DOA and frequency estimation for L-shaped array via compressed sensing PARAFAC method," *IEEE Access*, vol. 6, pp. 37204–37213, 2018.

[16] S. Uehashi, Y. Ogawa, T. Nishimura, and T. Ohgane, "Prediction of time-varying multi-user MIMO channels based on DOA estimation using compressed sensing," *IEEE Trans. Veh. Technol.*, vol. 68, no. 1, pp. 565–577, Jan. 2019.

[17] J. Tropp and A. C. Gilbert, "Signal recovery from partial information via orthogonal matching pursuit," *IEEE Trans. Inf. Theory*, vol. 53, no. 12, pp. 4655–4666, Dec. 2007.

[18] H. Li and G. Liu, "An improved analysis for support recovery with orthogonal matching pursuit under general perturbations," *IEEE Access*, vol. 6, pp. 18856–18867, 2018.

[19] G. Tzagkarakis, P. Tsakalides, and J.-L. Starck, "Covariation-based subspace-augmented MUSIC for joint sparse support recovery in impulsive environments," *Signal Process.*, vol. 93, no. 5, pp. 1365–1373, May 2013.
[20] J. A. Tropp, J. N. Laska, M. F. Duarte, J. K. Romberg, and R. G. Baraniuk, "Beyond Nyquist: Efficient sampling of sparse bandlimited signals," *IEEE Trans. Inf. Theory*, vol. 56, no. 1, pp. 520–544, Jan. 2010.
[21] G. Shi, J. Lin, X. Chen, F. Qi, D. Liu, and L. Zhang, "UWB echo signal detection with ultra-low rate sampling based on compressed sensing," *IEEE Trans. Circuits Syst., II, Exp. Briefs*, vol. 55, no. 4, pp. 379–383, Apr. 2008.
[22] M. Mishali and Y. C. Eldar, "From theory to practice: Sub-Nyquist sampling of sparse wideband analog signals," *IEEE J. Sel. Topics Signal Process.*, vol. 4, no. 2, pp. 375–391, Apr. 2010.
[23] Y. J. Zhao, Y. H. Hu, and H. J. Wang, "Enhanced random equivalent sampling based on compressed sensing," *IEEE Trans. Instrum. Meas.*, vol. 61, no. 3, pp. 579–586, Mar. 2012.
[24] Y. Zhao, Y. H. Hu, and J. Liu, "Random triggering-based sub-Nyquist sampling system for sparse multiband signal," *IEEE Trans. Instrum. Meas.*, vol. 66, no. 7, pp. 1789–1797, Jul. 2017.
[25] T. Haque, R. T. Yazicigil, K. J.-L. Pan, J. Wright, and P. R. Kinget, "Theory and design of a quadrature analog-to-information converter for energy-efficient wideband spectrum sensing," *IEEE Trans. Circuits Syst. I, Reg. Papers*, vol. 62, no. 2, pp. 527–535, Feb. 2015.
[26] N. Fu, G. Huang, L. Zheng, and X. Wang, "Sub-Nyquist sampling of multiple sinusoids," *IEEE Signal Process. Lett.*, vol. 25, no. 4, pp. 581–585, Apr. 2018.
[27] N. Fu, J. Gao, G. Huang, Z. Wei, and L. Qiao, "Parameter measurement of M-Ary PSK signals with finite rate of innovation," *IEEE Trans. Instrum. Meas.*, vol. 68, no. 5, pp. 1271–1283, May 2019.
[28] P. P. Vaidyanathan and P. Pal, "Sparse sensing with co-prime samplers and arrays," *IEEE Trans. Signal Process.*, vol. 59, no. 2, pp. 573–586, Feb. 2011.
[29] L. Xiao and X.-G. Xia, "Frequency determination from truly sub-Nyquist samplers based on robust Chinese remainder theorem," *Signal Process.*, vol. 150, pp. 248–258, Sep. 2018.
[30] D. D. Ariananda and G. Leus, "Compressive wideband power spectrum estimation," *IEEE Trans. Signal Process.*, vol. 60, no. 9, pp. 4775–4789, Sep. 2012.
[31] D. D. Ariananda and G. Leus, "Power spectrum blind sampling," *IEEE Signal Process. Lett.*, vol. 18, no. 8, pp. 443–446, Aug. 2011.
[32] Y. Zhao, H. Wang, X. Zhuang, Z. Dai, and H. Wu, "Frequency domain sensing system using random modulation pre-integrator," *IET Sci., Meas. Technol.*, vol. 7, no. 3, pp. 166–170, May 2013.

YIJIU ZHAO (M'12) received the B.S. and M.S. degrees in automation engineering and the Ph.D. degree in measuring and testing technology and instruments from the University of Electronic Science and Technology of China (UESTC), Chengdu, China, in 2004, 2007, and 2012, respectively, where he is currently an Associate Professor with the School of Automation Engineering.

His research interests include compressed sensing, signal processing, and analog signal sampling.

YU CHEN received the B.S. degree in electronical engineering from the University of Electronic Science and Technology of China, China, in 2017, where he is currently pursuing the M.S. degree with the School of Automation Engineering. His research interests include signal processing and compressive sampling.

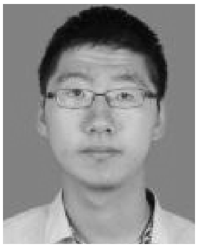

YANZE ZHENG received the B.S. degree in electronical engineering from Southwest Petroleum University, China, in 2017. He is currently pursuing the Ph.D. degree with the School of Automation Engineering, University of Electronic Science and Technology of China. His research interests include signal processing, instrumentation, and measurement.

YI ZHUANG received the B.S. degree in electronical engineering from the Tianjin University of Science and Technology, China, in 2018. She is currently pursuing the M.S. degree with the School of Automation Engineering, University of Electronic Science and Technology of China. Her research interests include signal processing and compressive sampling.

WEIFENG WEN received the B.S. and M.S. degrees in automation engineering from the University of Electronic Science and Technology of China, Chengdu, China, in 2004 and 2007, respectively.

He is currently an Associate Researcher with the Institute of Fluid Physics, China Academy of Engineering Physics, China. His research interests include instrumentation measurement and analog signal sampling.